第33卷 第6期 焊 接 学 报 Vol. 33 No. 6
2012年6月 TRANSACTIONS OF THE CHINA WELDING INSTITUTION June 2012

热输入对800 MPa级超厚板窄间隙焊缝金属组织和性能的影响

魏金山， 齐彦昌， 彭 云， 田志凌
(钢铁研究总院 先进钢铁流程及材料国家重点实验室，北京 100081)

摘 要：采用三种热输入进行超厚板窄间隙熔化极气体保护焊，借助金相显微镜、扫描电子显微镜及附带EDS系统和透射电子显微镜研究了热输入对焊缝金属组织和性能的影响. 结果表明，三种热输入焊缝金属组织主要由板条马氏体、无碳化物贝氏体、M-A组元和残余奥氏体组成. 随着焊接热输入的增加，焊缝组织中马氏体含量减少；也使无碳化物贝氏体形核率降低，造成无碳化物贝氏体粗化. 并且当贝氏体相变时热输入的增加使碳原子扩散距离变远，促使残余奥氏体形状由膜状向块状转变. 另外随着热输入的增加，焊缝金属强度下降，而冲击韧性对热输入不敏感.

关键词：热输入；焊缝金属；组织；性能
中图分类号：TG142.2 **文献标识码**：A **文章编号**：0253-360X(2012)06-0031-04

魏金山

0 序 言

近年来海洋工程、管线钢和压力容器等各种大型焊接结构推广使用强度高于780 MPa钢材[1-3]，而研究其配套的焊缝金属的组织和性能显得十分重要. 为了确保高强钢接头的力学性能和降低建造成本，控制焊缝金属组织和生产效率是非常关键的因素. 尤其高强钢超厚板的焊接，这些问题就更加突出.

一般来说性能取决于组织，而组织取决于焊缝金属的化学成分及冷却速度[4,5]. 焊缝金属的化学成分依赖于母材的成分、焊接材料的成分、稀释率和焊接时的电弧反应. 冷却速度取决于热输入、板厚、预热温度等. 当焊接材料及母材都已经确定后，焊缝金属的组织和性能由焊接工艺条件来决定. 其中热输入是集中反映电流、电压和焊接速度的综合指标，是决定焊缝金属组织和性能的最重要的因素之一. 热输入不但影响到冷却速度，而且对焊缝金属的化学成分也有影响，所以研究热输入对高强钢超厚板窄间隙焊接有十分重要的意义.

文中试板坡口为窄间隙，利用气体保护焊进行焊接，采用工程上横焊、平焊和立焊实际使用的三种热输入，并研究热输入对焊缝组织和性能的影响.

收稿日期：2011-04-08
基金项目：国家863高技术研究发展计划资助项目(2007AA03A207)

1 试验方法

试板选用10Ni5CrMoV钢，尺寸为500 mm×175 mm×100 mm，坡口设计如图1所示. 三种热输入均采用同一种焊丝，焊丝为自行设计冶炼的Mn-Ni-Cr-Mo系实心焊丝，直径1.2 mm. 焊接方法采用熔化极气体保护焊，直流反接，保护气体为95% Ar和5% CO_2混合气体，道间温度100～120 ℃. 采用17，20和23 kJ/cm三种热输入进行焊接. 试板及焊缝金属化学成分见表1.

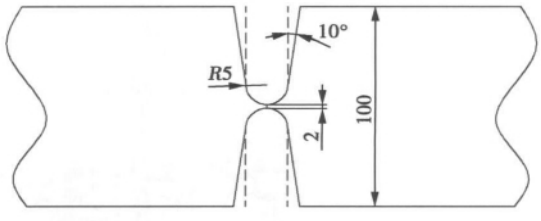

图1 坡口示意图(mm)

Fig. 1 Schematic diagram of groove

表1 母材及焊丝的主要化学成分(质量分数，%)

Table 1 Chemical compositions of base metal and weld wire

	C	Si	Mn	Cr	Mo	Ni	Fe
焊丝	0.055	0.52	1.88	0.38	0.74	2.44	余量
母材	0.072	0.18	0.57	0.60	0.50	5.13	余量

焊缝金属用砂纸研磨、抛光后，用 3% 的硝酸酒精显示基体组织，依据文献 [5] 介绍的腐蚀方法来显示 M-A 组元. 利用 LeicaMEF-4M 光学显微镜及 SCIAS6.0 图像分析系统研究焊缝金属的微观组织. 透射试样片用 800 号砂纸磨到 50 μm 以下，用 MTP-1A 磁力减薄器电解双喷减薄，减薄液为 6% 高氯酸乙醇溶液，温度 -25 ℃，电压 25 V，电流 60 mA. 采用 H-800 透射电镜研究焊缝金属的微观精细结构.

拉伸和冲击样坯按照国家标准 GB2649—1989《焊接接头机械性能试验取样方法》进行取样. 拉伸试样尺寸为 ϕ 10 mm × 105 mm，并按照国家标准 GB 2562—1989《焊缝及熔敷金属拉伸试验方法》进行拉伸试验. 冲击试样为 V 形缺口，试样尺寸为 10 mm × 10 mm × 55 mm，按照国家标准 GB/T2650—1989《焊接接头冲击试验方法》进行冲击试验.

2 试验结果与讨论

2.1 热输入对焊缝金属组织的影响

图 2 是三种热输入下焊缝金属的显微组织，可以看出在光学显微镜下三种焊缝金属的组织类型基本相似，均是板条结构. 并且部分板条束呈“交织状，对比三种焊缝发现，随着热输入的增大，组织粗化. 由于光学显微镜的分辨率较低，观察更为精细结构受到了限制. 进而借助高分辨率的透射电镜观察焊缝金属组织结构，研究发现三种焊缝金属组织比较接近，主要由板条马氏体、无碳化物贝氏体和残余奥氏体组成，如图 3 ~ 图 6 所示. 可以看出在光学显微镜下呈“交织状”组织为无碳化物贝氏体，并且随着热输入的增加无碳化物贝氏体板条越来越粗大，如图 3 所示. 另外在热输入 17 kJ/cm 和 20 kJ/cm焊缝金属中残余奥氏体呈长条状，而在热输入 23 kJ/cm 焊缝金属中出现块状残余奥氏体，如图 4 所示. 同时在焊缝金属中发现 M-A 组元，如图 5 所示. 图 5a 中白色的亮点为 M-A 组元，白色带状区域组织为马氏体，通过透射观察发现 M-A 组元尺寸比较小，如图 5b 所示，这种小尺寸 M-A 组元对韧性影响较小 [7]. 最后借助 Lepera 试剂腐蚀三种焊缝金属发现马氏体含量不同，分别为 10.3%，9% 和 6%. 图 6b 是 Lepera 试剂腐蚀热输入 23 kJ/cm 焊缝金属后金相照片，白色为马氏体.

通过上面论述可以知道，随着热输入的增大，贝氏体板条越来越粗大. 这是因为热输入小意味着冷却速度快，过冷度 ΔT 大，相变温度下降，新旧两相自由能差增大，临界晶核尺寸减小，所需要的临界晶核形成功减小，使形核率增加，因此冷却速度快导致

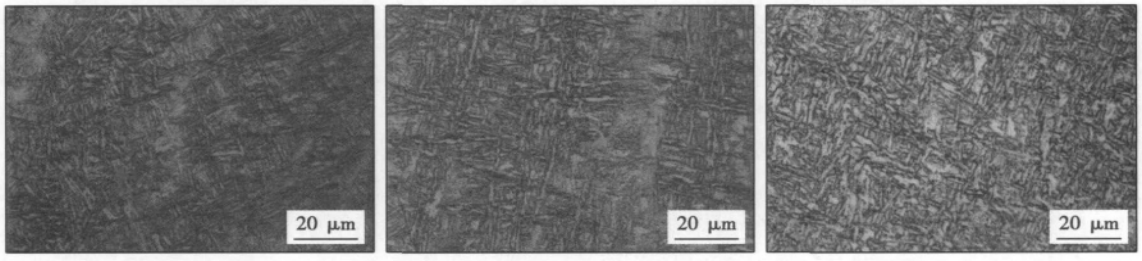

(a) 热输入17 kJ/cm (b) 热输入20 kJ/cm (c) 热输入23 kJ/cm

图 2 三种热输入的焊缝显微组织

Fig. 2 Microstructures of weld metal welded with three heat inputs

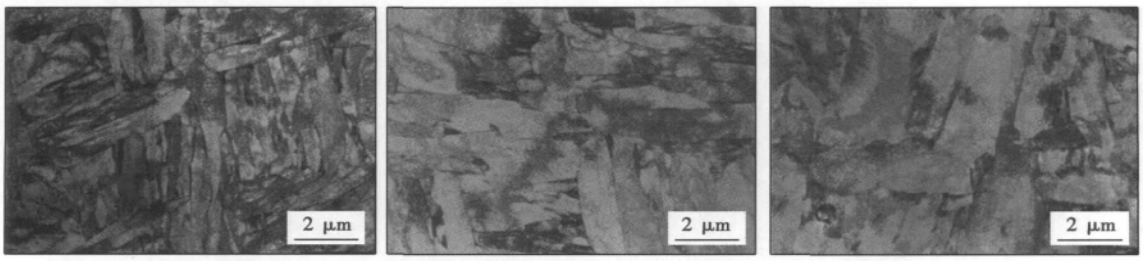

(a) 热输入17 kJ/cm (b) 热输入20 kJ/cm (c) 热输入23 kJ/cm

图 3 三种热输入焊缝中的无碳化物贝氏体

Fig. 3 Carbide free bainite of weld metal with three heat inputs

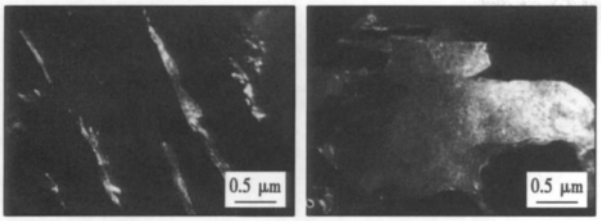

(a) 热输入20 kJ/cm　　(b) 热输入23 kJ/cm

图 4　不同热输入焊缝金属中奥氏体形貌(暗场相)

Fig. 4　Appearance of austenite in weld metal with different heat inputs

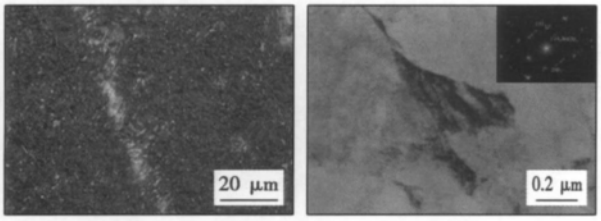

(a) 金相　　(b) 透射

图 5　热输入 23 kJ/cm 焊缝金属中的 M-A 组元

Fig. 5　M-A constituent in weld metal welded with 23 kJ/cm heat input

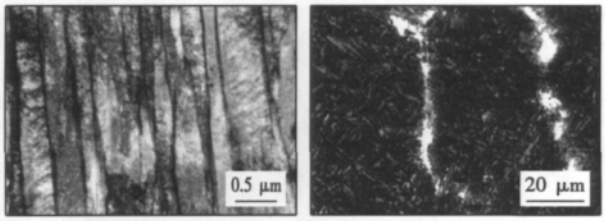

(a) 透射　　(b) Lepera试剂腐蚀后金相组织

图 6　热输入 23 kJ/cm 焊缝组织中的马氏体

Fig. 6　Martensite in weld metal welded with 23 kJ/cm heat input

贝氏体板条细小,形核率表达式为

$$N = C_0 \exp\left(-\frac{\Delta G^*}{RT}\right) \tag{1}$$

式中: N 为贝氏体形核率; C_0 为常数; ΔG^* 为临界形核功; R 为气体常数; T 为温度.

随着热输入的增大,熔池内化学反应更加剧烈,Mn,Si,Ti 等合金元素烧损增加,导致焊缝金属贝氏体相变温度 T_{Bs} 升高. 另一方面,冷却速度越快,贝氏体相变温度越低[8],因此冷却速度更加加大了三种焊缝金属 T_{Bs} 差距. 当热输入小时,合金元素烧损小,冷却速度快,因而贝氏体相变温度较低. 当发生贝氏体转变时 C 原子的扩散速率较慢,而且扩散时间短,使碳不能向远处的奥氏体内扩散,所以 C 原子聚集在 α/γ 界面附近,碳浓度梯度大,如图 7 所示[9]. 当 α/γ 界面附近 C 原子浓度达到一定程度时,贝氏体停止生长. 而此时在贝氏体板条间形成一层薄薄富碳奥氏体膜,另外由于焊缝金属中含有一定量的 Si 元素,富碳奥氏体中渗碳体析出受到抑制[10]. 最终这层奥氏体膜保留至室温如图 4a 所示.

当热输入较大时焊缝金属贝氏体转变温度 B_s 高,此时 C 原子的扩散速率较快,而且扩散时间长,碳能够向未转变奥氏体内更远处扩散,所以 C 元素浓度梯度相对较小,如图 7 所示. 随着贝氏体的生长,C 原子不断的向未转变的奥氏体内聚集,并且向远处扩散,这样使更大范围内未转变奥氏体内碳含量高. 当奥氏体内碳达到一定程度时,贝氏体停止生长,此时形成富碳块状奥氏体.

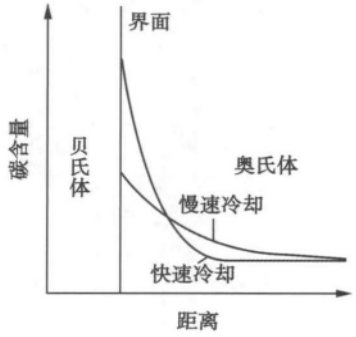

图 7　α/γ 界面附近 C 元素浓度梯度示意图

Fig. 7　Schematic diagram showing carbon gradients adjacent to austenite-ferrite interface

2.2　热输入对焊缝金属力学性能的影响

从图 8a 中可以看出随着热输入的增加抗拉强度略有下降,而屈服强度下降趋势明显,由 890 MPa 下降到 800 MPa. 通过前面分析可以知道组织主要由马氏体和无碳化物贝氏体组成,这两种组织含量随着热输入的增大发生了变化,一方面马氏体含量随着热输入的增大越来越少,另一方面无碳化物贝氏体随着热输入的增大而粗化,这两方面的原因导致了随着热输入的增大焊缝金属强度降低.

图 8b 是不同热输入下焊缝金属系列温度冲击吸收功曲线,可以看出三种焊缝金属随着试验温度的降低,冲击功均显示下降的趋势. 并且发现在同一试验温度,不同热输入焊缝的冲击吸收功接近. 这意味着热输入在 17 ~ 23 kJ/cm 范围内焊缝金属的冲击韧性对热输入不敏感.

三种热输入焊缝金属冲击断口形貌基本相似. 以热输入 20 kJ/cm 焊缝金属在 −50 ℃冲击断口为例. 微裂纹首先在缺口处萌生,并且稳定扩展形成

灰暗色的纤维状形貌，裂纹稳定扩展一定距离后裂纹发生失稳形成结晶状形貌. 纤维区发现分布大量韧窝，它们均以微孔聚集型方式断裂，如图 9a 所示. 韧窝内存在夹杂物，经 EDS 分析夹杂物为钛，铝，硅，锰和铁的复合氧化物. 晶状区以解理断裂和微孔聚集型混合模式断裂，如图 9b 所示.

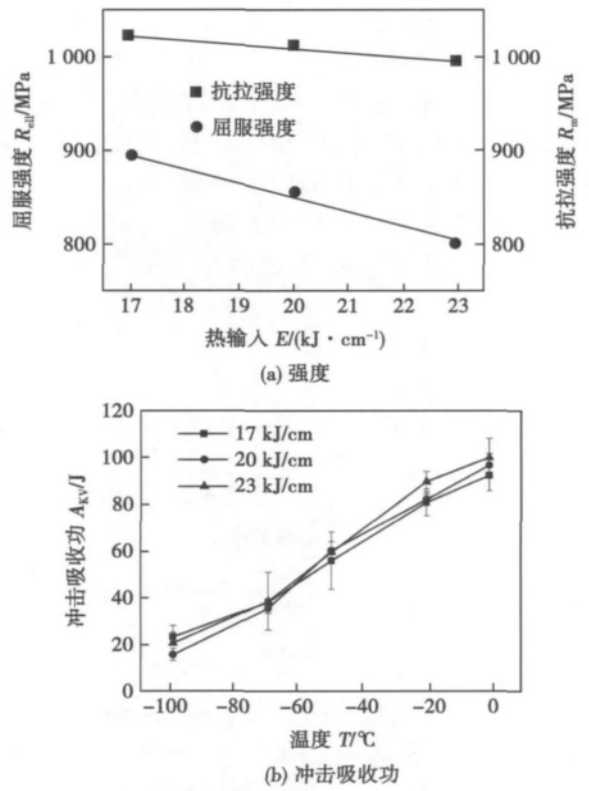

图 8 热输入对力学性能的影响

Fig. 8 Effect of heat input on properties

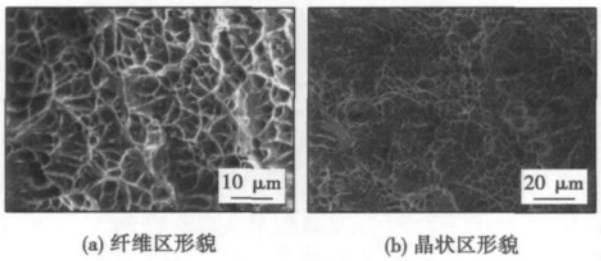

图 9 热输入为 20 kJ/cm 焊缝金属冲击断口形貌(−50 ℃)

Fig. 9 Impact fracture surface of weld metal

3 结 论

(1) 焊缝金属主要由板条马氏体、无碳化物贝氏体，M-A 组元和残余奥氏体组成. 随着热输入的增加，焊缝组织中马氏体含量减少.

(2) 随着热输入的增加，无碳化物贝氏体形核率降低，造成无碳化物贝氏体粗大.

(3) 随着热输入的增加，焊缝金属冷却速度变慢，贝氏体相变温度 T_{Bs} 升高，在贝氏体转变时 C 原子扩散距离变远，促使残余奥氏体形状由膜状向块状转变.

(4) 随着热输入的增加，焊缝金属强度下降. 冲击韧性对热输入不敏感.

参考文献:

[1] Gouda M, Takahashi M, Ikeuchi K. Microstructures of gas metal arc weld metal of 950 MPa class steel [J]. Science and Technology of Welding and Joining, 2005, 10(3): 369 - 377.

[2] 冯 伟，曹 睿，彭 云，等. 980 MPa 级高强钢焊接接头 HAZ 的组织和性能 [J]. 焊接学报，2009，30(7)：17 - 20.
Feng Wei, Cao Rui, Peng Yun, *et al*. Microstructure and mechanical properties of HAZ of 980 MPa high strength steel joints [J]. Transactions of the China Welding Institution, 2009, 30(7): 17 - 20.

[3] 齐彦昌，彭 云，魏金山，等. 碳对 C-1.5Mn-2.5Ni-0.5Cr-0.5Mo 高强钢焊缝金属组织和性能的影响 [J]. 焊接学报，2010，31(11)：41 - 44.
Qi Yanchang, Peng Yun, Wei Jinshan, *et al*. The effect of carbon on microstructures and properties of the C-1.5Mn-2.5Ni-0.5Cr-0.5Mo high strength steel weld metal [J]. Transactions of the China Welding Institution, 2010, 31(11): 41 - 44.

[4] Oldland P T, Ramsay C W, Matlock D, *et al*. Significant features of high-strength steel weld metal microstructures [J]. Welding Journal, 1989, 68(4): 158s - 168s.

[5] 张德勤，田志凌，杜则裕，等. 热输入对 X65 钢焊缝金属组织及性能的影响 [J]. 焊接学报，2001，22(5)：31 - 34.
Zhang Deqin, Tian Zhiling, Du Zeyu, *et al*. Effect of heat input on microstructure and properties of weld metal in X65 steel [J]. Transactions of the China Welding Institution, 2001, 22(5): 31 - 34.

[6] Alé R M, Rebello J M A, Charlier J. A metallographic technique for detecting martensite-austenite constituents in the weld heat-affected zone of a micro-alloyed steel [J]. Materials Characterization, 1996, 37(2/3): 89 - 93.

[7] 赵 琳，张旭东，陈武柱. 800 MPa 级低合金钢焊接热影响区韧性的研究 [J]. 金属学报，2005，41(4)：392 - 396.
Zhao Lin, Zhang Xudong, Chen Wuzhu. Toughness of heat-affected zone of 800 MPa grade low alloy steel [J]. Acta Metallurgica Sinica, 2005, 41(4): 392 - 396.

[8] Manabu T. Bainite transformation under continuous cooling of Nb-microalloyed low carbon steel [J]. Journal of Iron and Steel Research International, 2006, 13(3): 36 - 39.

[9] Biss V, Cryderman R L. Martensite and retained austenite in hot-rolled low-carbon bainitic steels [J]. Metallurgical Transactions, 1971, 2(8): 2267 - 2276.

[10] Bhadeshia H K D H, Edmonds D V. The bainite transformation in a silicon steel [J]. Metallurgical Transactions A, 1979, 10(7): 895 - 907.

作者简介: 魏金山，男，1962 年出生，博士，教授级高级工程师. 主要从事焊接材料研发及焊接工艺性. 发表论文 20 余篇. Email: weijinshan@nercast.com

ellipsoid heat source was employed to simulate the metal-inert gas welding. The measured as-welded deflection data of ten real rail floors at the production site was highly coincident with the numerical simulation results. The results proved that, the thermo-mechanical coupling analysis and the dynamic material properties were two essential factors in the high precision simulation of high speed rail floor, which could lay a digital workplace for the improvement of the current process and further development of the new-type assembly.

Key words: high speed rail floor; hollow extruded shape of aluminum alloy; as-welded deflection; thermo-mechanical coupling

Influence of Zn addition on wettability of AgCu brazing alloy on TiC cermet LEI Min, ZHANG Lixia, LI Hongwei, FENG Jicai (State Key Laboratory of Advanced Welding and Joining, Harbin Institute of Technology, Harbin 15001, China). pp 19 – 22

Abstract: Wetting experiments of AgCu eutectic brazing alloy and AgCuZn brazing alloy with 30wt.% Zn addition were performed on TiC cermet. Based on observation of wetting angles of the two brazing alloys on the cermet and interfacial microstructure, it is found that wettability of brazing alloy on TiC cermet is greatly improved by Zn addition. When AgCu brazing alloy was adopted, the microstructure was Ag(s.s) + Cu(s.s) /(Cu,Ni) + Ag(s.s) /TiC cermet + Ag(s.s) + Cu(s.s) /TiC cermet from the near exterior surface of the alloy to the cermet. However, when Zn was added into AgCu brazing alloy, the microstructure was Ag(s.s) + Cu(s.s) + (Cu,Ni) /Ag(s.s) + Cu(s.s) /(Cu,Ni) /TiC cermet + Ag(s.s) + Cu(s.s) /TiC cermet. And it's shown that evaporation of Zn in the vacuum improves dissolution and diffusion of Ni at the interface and the wetting angle of the brazing alloy on the cermet decreases from 120.6° to 33.9°.

Key words: wettability; microstructure; cermet; brazing alloy

Interfacial characteristic and property of Ti/Al dissimilar alloys joint with arc welding-brazing LV Shixiong[1], JING Xiaojun[1], HUANG Yongxian[1], CHENG Jinli[2], ZHENG Chuanqi[1] (1. State Key Laboratory of Advanced Welding and Joining, Harbin Institute of Technology, Harbin 150001, China; 2. Xi'an Space Engine Factory, Xi'an 710100, China). pp 23 – 26

Abstract: Ti/Al dissimilar alloys were successfully joined by AlSi5 filler metal and TIG-AC arc, and the joints with the characters welding and brazing were gained. The interfacial microstructure and property of Ti/Al welding brazing joints were analyzed by optical microscope (OM), scanning electron microscopy (SEM), energy dispersive X-ray spectrometer (EDS) and tensile test. The results indicate that interfacial layers exhibit club-shaped, diamond-shaped and coniform-shaped respectively, with welding current changes from 30 A to 60 A. The excessive heat input resulted in oversized column interfacial layer, cold cracks were produced during cooling stage under influence of welding stress. $TiAl_3$ is the main phase of the interfacial layer, which is a typical supersaturated solid solution of Si element. The strength-current curve exhibits two peak values. The maximum average tensile strength is 103 MPa with welding current of 30 A, while the curve exhibits the second peak value with welding current of 60 A due to the decreasing of arc energy density.

Key words: Ti/Al dissimilar alloys; arc welding brazing; intermetallic compound; mechanical property

Research of microstructure and mechanical behavior of welded joint of AZ91 magnesium alloy LIU Zhengjun, ZHAO Fudong, SU Yunhai, QI Yiuhong (Material Science and Engineering, Shenyang University of Technology, Shenyang 110000, China). pp 27 – 30

Abstract: The AC TIG was applied on AZ91 magnesium alloy plate(in 5mm thickness). The effect of different welding currents on microstructure and properties of surfacing layer was investigated by X-ray diffraction (XRD), Optical Microscope (OM), Scanning Electron Microscope (SEM), and Tensile Tester. The results show that with the increasing of welding current, the form of welding seam become bad and the grain growth get coarse. At the same time, gas porosity and crack are easy to by produced, which reduce the properties of the joint. The microstructure of the weld zone is composed of α-Mg matrix and β-Al12Mg17 phase. When the welding current is 100A, the mechanical properties of welded joints reach maximum, at this point tensile strength is 252 MPa, percentage elongation is 6.9%.

Key words: welding current; magnesium alloy; TIG; structure property

Effect of heat input on the microstructure and properties of weld metal welding in a 800 MPa grade heavy steel plate with narrow gap groove WEI Jinshan, QI Yanchang, PENG Yun, TIAN Zhilin (State Key Laboratory of Advanced Steel Processes and Products, Central Iron & Steel Research Institute, Beijing 100081, China). pp 31 – 34

Abstract: The heavy steel plates with narrow gap groove were welded by gas metal arc welding under three heat inputs, and the effects of heat input on microstructure and properties of the weld metal were investigated by means of optical microscopy, scanning electron microscopy with energy dispersive spectroscopy, and transmission electron microscopy. The results indicate that the microstructure of the three weld metal consist predominantly of lath martensite, carbide free bainite, M-A constituent and retained austenite. The amount of martensite decreases with the increasing of the heat input. As the heat input increases, bainite nucleation rate decreases, resulting in coarser bainite, and C diffuses the farther distance, resulting in variation of retained austenite morphology from strip to block. The strength of weld metal drops with the increasing of heat input, while the toughness is not sensitive to heat input.

Key words: heat input; weld metal; microstructure; properties

Loading pressure numerical analysis on radial friction lap welding joint of steel pipe ZHANG Yan[1], QIN Guoliang[2], ZHANG Chunbo[1], ZHOU Jun[1], ZHAO Yushan[1] (1. Harbin Welding Institute, China Academy of Machinery Science & Technology, Harbin 150080, China; 2. Institute of Advanced Welding Technology, Shandong University, Jinan 250061, China). pp 35 – 38